Supporting Information

Platinum Nanocatalyst Amplification: Redefining the Gold Standard for Lateral Flow Immunoassays with Ultrabroad Dynamic Range

Colleen N. Loynachan[†1], Michael R. Thomas[†1], Eleanor R. Gray[2], Daniel A. Richards[3], Jeongyun Kim[1], Benjamin S. Miller[2], Jennifer C. Brookes[2,4], Shweta Agarwal[1], Vijay Chudasama[3], Rachel A. McKendry[2], and Molly M. Stevens*[1]

†***Contributed equally***

1. Department of Materials, Department of Bioengineering and Institute of Biomedical Engineering, Imperial College London, London, SW7 2BP, UK

2. London Centre for Nanotechnology and the Division of Medicine, University College London, 17-19 Gordon Street, London, WC1H 0AH, UK

3. Department of Chemistry, University College London, 20 Gordon Street, London, WC1H 0AJ, UK

4. Department of Physics and Astronomy, University College London, 17-19 Gordon Street, London, WC1H 0AH, UK

Email: m.stevens@imperial.ac.uk

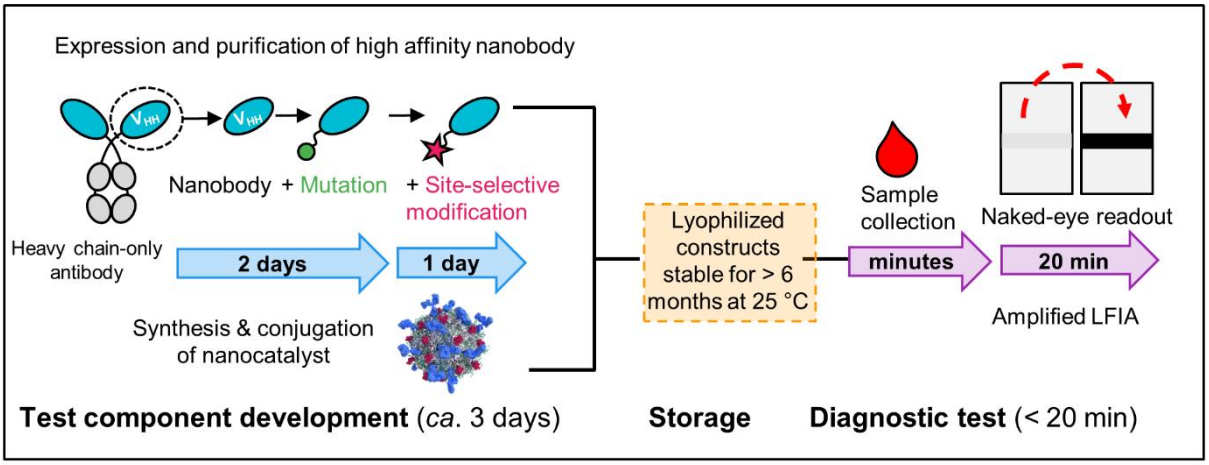

Supplementary Figure 1. Process flow for the rapid prototyping of amplified paper-based diagnostics for protein biomarkers, incorporating orthogonally modified nanobodies and highly active nanocatalyst labels.

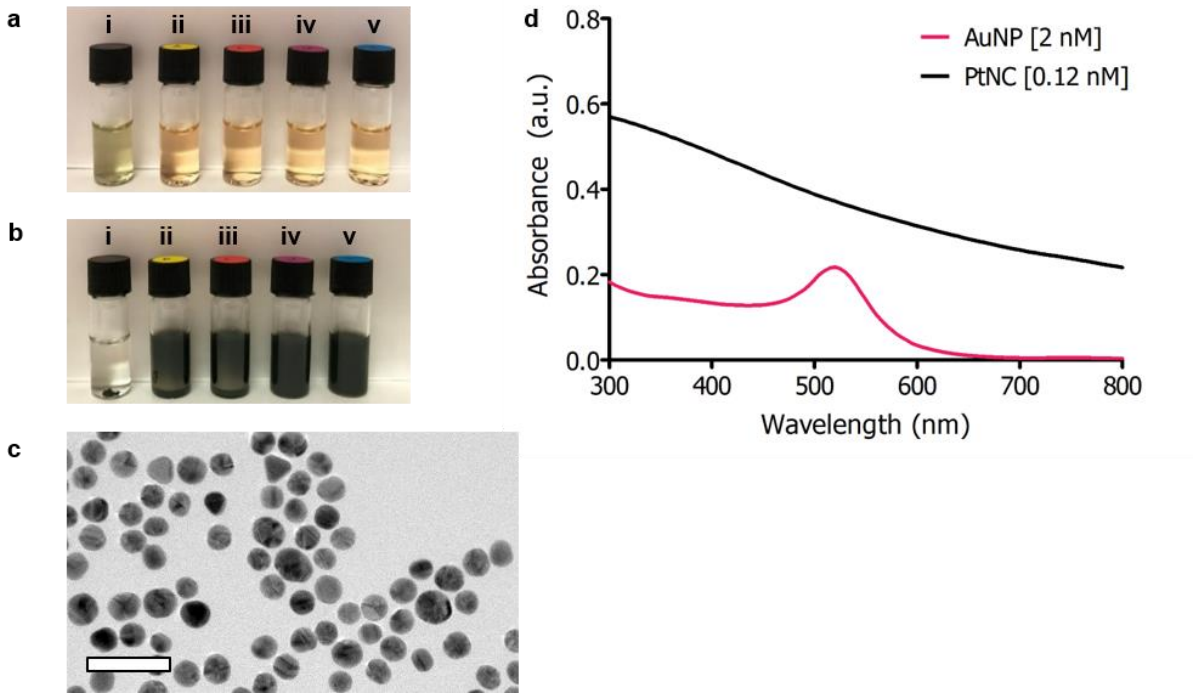

Supplementary Figure 2. Images of PtNC reaction components containing varying molecular weights of PVP: (i) no PVP, (ii) 3.5 kDa, (iii) 10 kDa, (iv) 29 kDa, (v) and 55 kDa; before (**a**) and after heat treatment (**b**) for 30 min at 65 °C. PtNCs synthesized in the absence of PVP aggregated and precipitated during reaction, indicating that PVP is critical for stabilization during reaction. Color change from light red to black indicates successful deposition of platinum on gold nanoparticle seeds. (**c**) TEM image of gold nanoparticle

seeds *ca*. 15 nm. Scale bar, 50 nm. (**d**) UV/Vis spectra of 15 nm gold nanoparticle seeds (2 nM, red) and *ca*. 90 nm PtNC (0.12 nM, black).

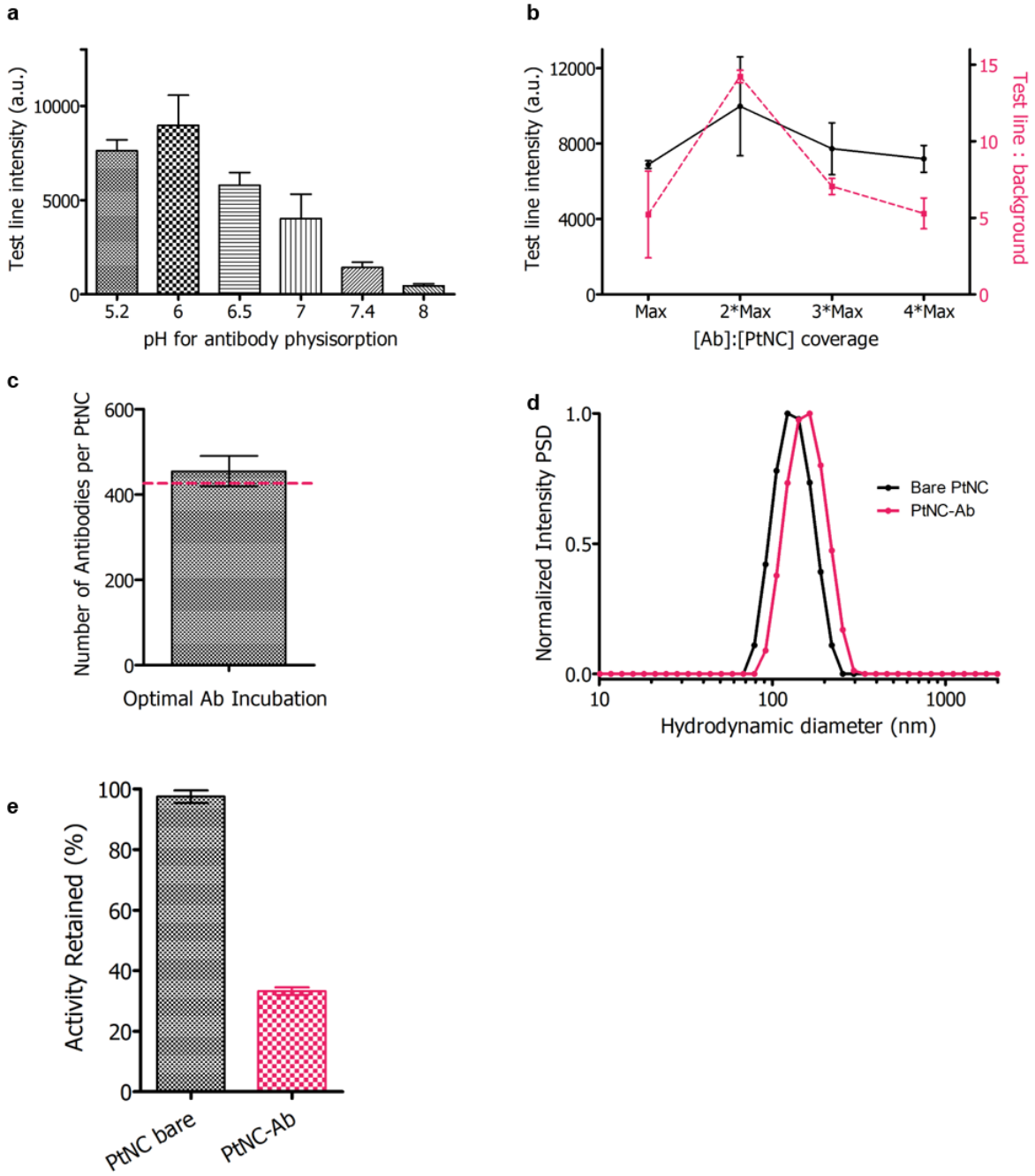

Supplementary Figure 3. (**a**) Plot of test line intensity against pH of antibody physisorption, showing the pH dependency of antibody conjugation, with pH 6 (pH adjusted using 10 mM HEPES buffer) being optimal. Physisorption is maximally achieved at a pH close to the isoelectric point of the protein to be conjugated. (**b**) Plot of test line intensity and “test line to background ratio” against varying antibody coverage on PtNCs. Antibody coverage densities

were calculated using the cross-sectional area of the antibody assuming a *ca*. 10 nm diameter protein, and surface area of PtNC sphere (using Z-average diameter from DLS). “Max” corresponds to the theoretical maximum number of antibodies that can pack onto the PtNC surface in a monolayer. The highest test line signal intensity was achieved when particles were conjugated in the presence of 2 times the “max” number of antibodies to theoretically saturate the surface. The signal was also quantified using the ratio of the intensity of the test line (for 50 $pg \cdot mL^{-1}$ spiked FBS) to the intensity of the test line for the blank sample (background). Test line signal intensity from the blank control sample indicates nonspecific binding. Test line to background ratio was highest at incubation with 2*max antibody coverage. Particles conjugated in less than an excess of antibodies resulted in PtNC aggregation during the conjugation, which led to elevated nonspecific binding in the blank sample and decreased test line to background ratio. (**c**) The number of antibodies conjugated to PtNCs (*ca*. 120 nm diameter) after incubation of a fixed particle concentration in optimal antibody coverage solution (2*max) for 3 h. When PtNCs are incubated in a 2-fold excess of antibodies with respect to surface area, a monolayer is formed. Red dotted line indicates the theoretical number of antibodies to fully coat PtNCs. After antibody modification, the particles were centrifuged and the concentration of antibody in the supernatant (unbound fraction) was measured using a Thermo Scientific Micro-BCA (bicinchoninic acid) Protein Assay Kit. (**d**) DLS measurements showing normalized particle size distribution (intensity) for bare PtNCs (black) and antibody modified PtNCs (red). (**e**) Percent of activity retained for PtNCs which have been modified with antibodies and subsequently blocked in 2 wt% beta-casein blocking solution. Antibody modified particles retain *ca*. 35% activity compared to as-synthesized PtNCs. All data are averaged from ≥ 3 independent measurements where error bars represent the standard deviation from the mean.

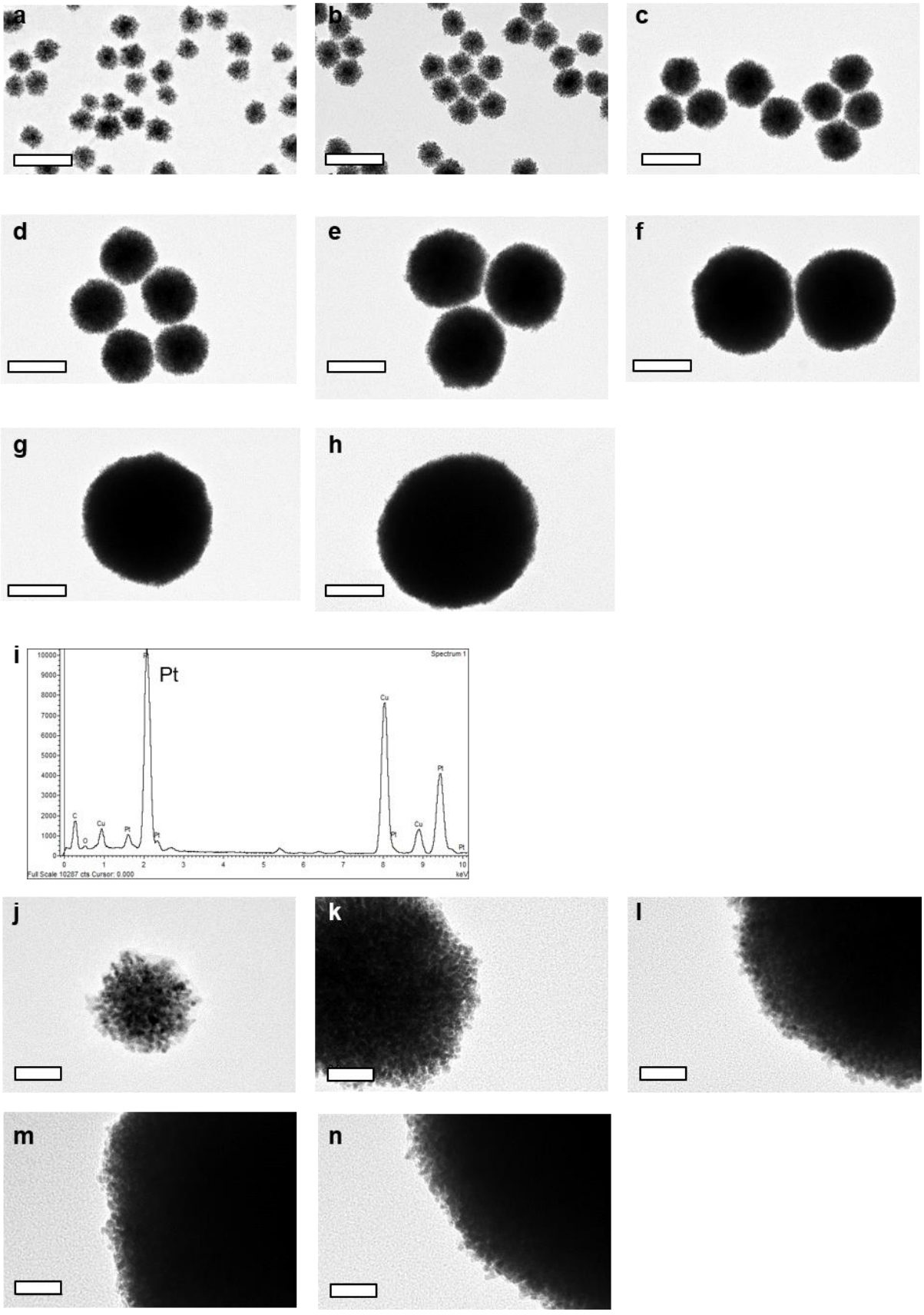
a
b
c
d
e
f
g
h
i
Pt
Spectrum 1
C
O
Cu
Pt
Cu
Pt
Full Scale 10287 cts Cursor: 0.000
keV
j
k
l
m
n

Supplementary Figure 4. TEM images of PtNCs formed by varying [Au]: [Pt]. Batches were synthesized in presence of different gold nanoparticle seed concentrations: (**a**) 5 nM, (**b**) 2.5 nM, (**c**) 0.6 nM, (**d**) 0.3 nM, (**e**) 150 pM *ca*. 120 nm PtNCs as seeds, (**f**) 75 pM *ca*. 120 nm PtNCs as seeds, (**g**) 40 pM *ca*. 120 nm PtNCs as seeds, (**h**) 20 pM *ca*. 120 nm PtNCs as seeds. Scale bars **a-h**, 100 nm. (**i**) Representative EDS spectra of an individual PtNC from the synthesized PtNCs shown in (d) indicating the presence of platinum in the PtNC shell. Nanoscale roughness of PtNCs produced using seeded synthesis for particles of average diameter measured by DLS (number distribution): (**j**) 50 nm, (**k**) 120 nm, (**l**) 180 nm, (**m**) 215 nm, (**n**) 280 nm. Scale bars **j-n**, 20 nm.

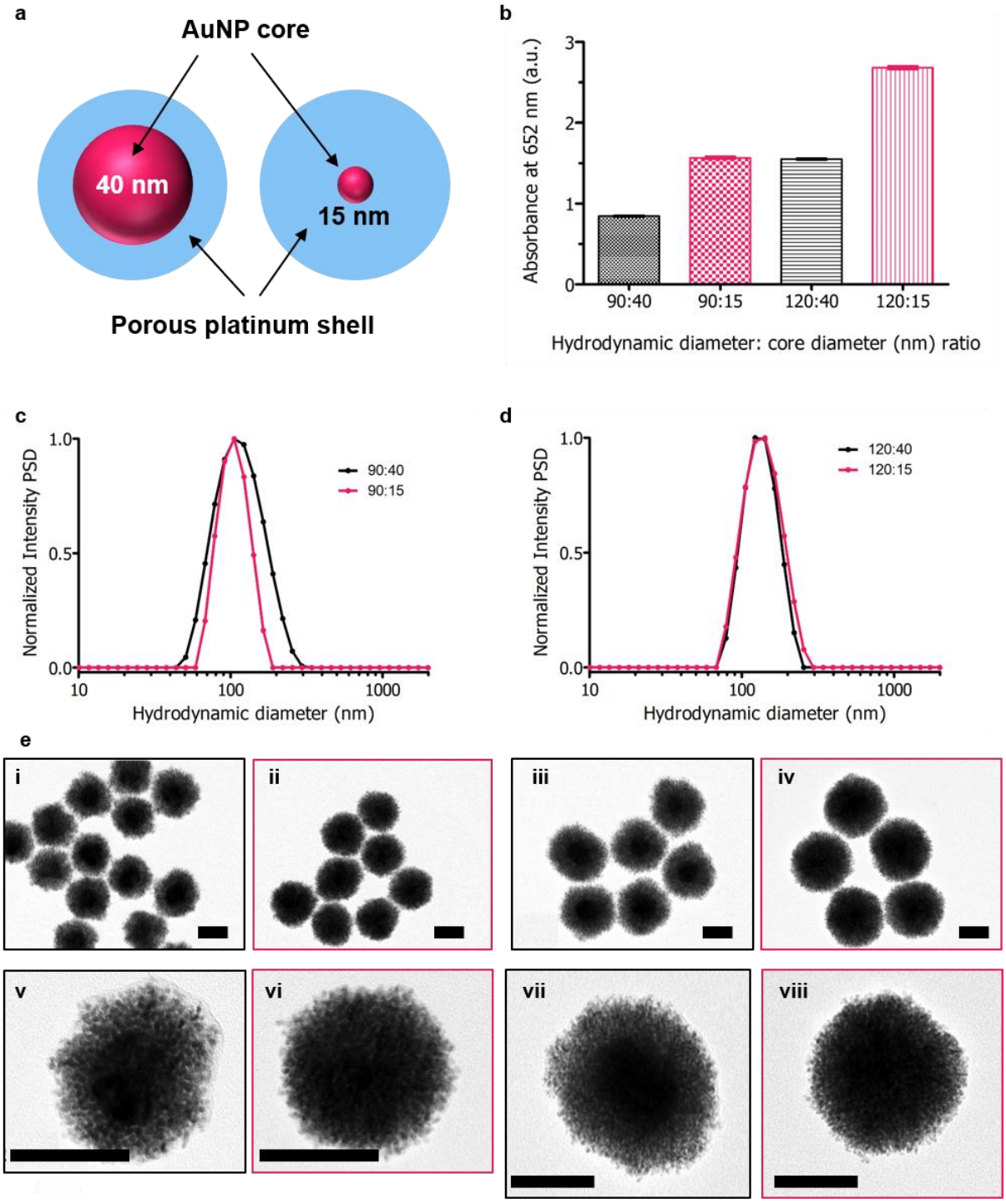

Supplementary Figure 5. (**a**) Schematic illustration of PtNCs synthesized using two different AuNP core sizes: 40 nm and 15 nm. By maintaining the external hydrodynamic diameter of the particle but varying the core size (red), we can effectively modulate the thickness of the porous shell (blue). (**b**) Catalytic activity measured by the absorbance at 652 nm corresponding to the oxidation of TMB by H_2O_2 for 90 nm and 120 nm PtNCs synthesized using 40 nm (black) or 15 nm (red) core sizes. Error bars represent standard

deviation from three independent experiments. For both hydrodynamic sizes, the PtNCs synthesized with 15 nm cores exhibit higher activity, due to the increase in porous shell volume compared PtNCs of equivalent external diameter with 40 nm core. DLS measurements showing normalized particle size distribution (intensity) for (**c**) *ca.* 90 nm or (**d**) 120 nm external diameter with either 15 nm (red) or 40 nm (black) AuNP core diameter. (**e**) TEM images of PtNCs with varying hydrodynamic diameter to core diameter ratio: (i, v) 90:40, (ii, vi) 90:15, (iii, vii) 120:40, and (iv, viii) 120:15 (nm). Scale bar is 50 nm.

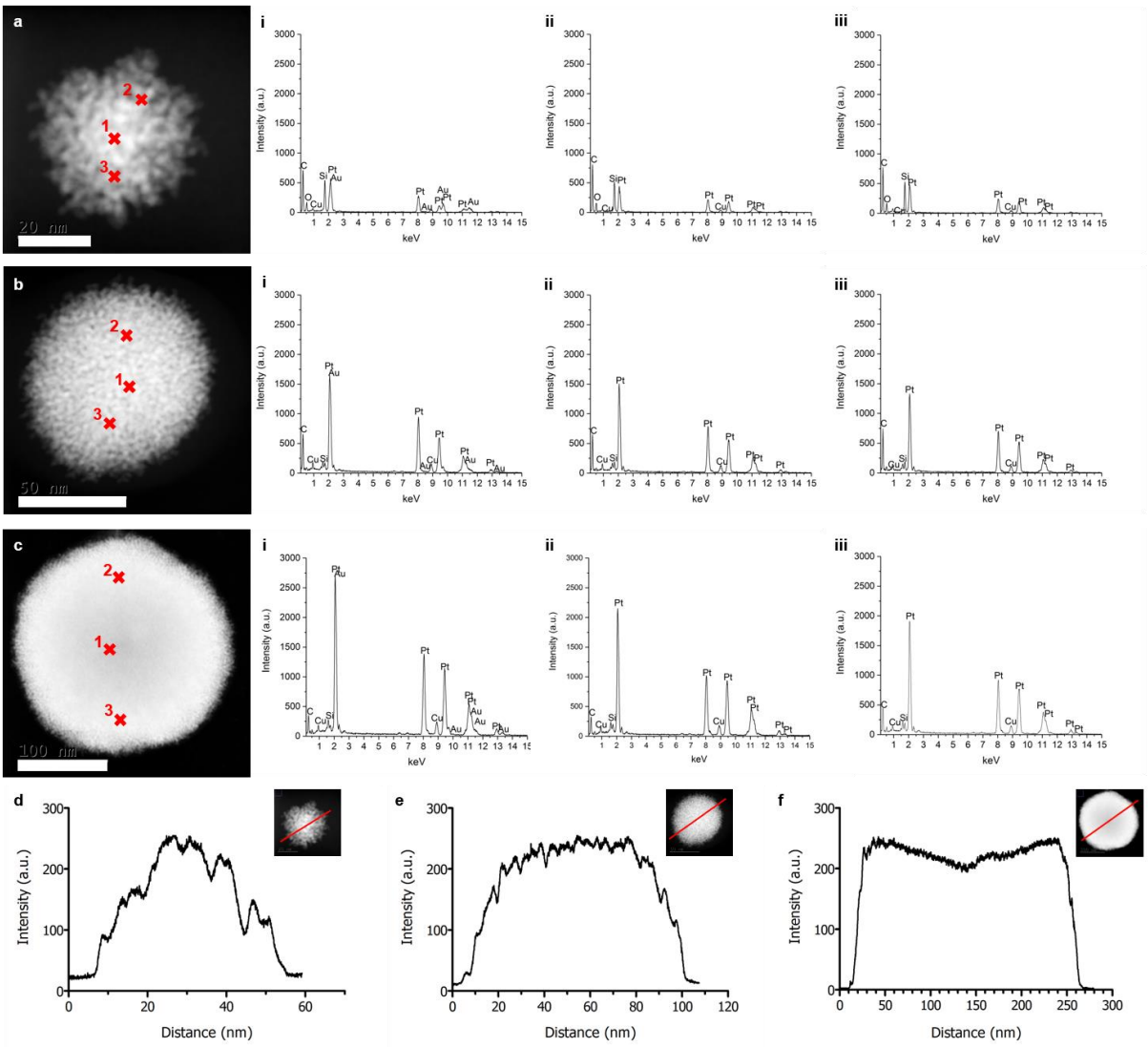

Supplementary Figure 6. High-angle annular dark-field STEM (HAADF-STEM) images of (**a**) *ca.* 50 nm (scale bar, 20 nm), (**b**) 100 nm (scale bar, 50 nm), and (**c**) 200 nm (scale bar, 100 nm) PtNCs with corresponding Energy Dispersive X-ray point spectra (EDS) (i – iii). Au

is observed in the core for all sizes, while Pt is confined to the shell, confirming the core-shell structure. The contrast in HAADF-STEM is sensitive to the atomic (Z) number contrast and therefore dark contrast regions in particles highlight the porosity within the Pt shell. Intensity line profiles across HAADF images for (**d**) 50 nm, (**e**) 100 nm, and (**f**) 200 nm PtNCs. Higher density platinum (lower porosity) is observed at the periphery of 200 nm PtNCs produced through a layer-by-layer synthesis approach.

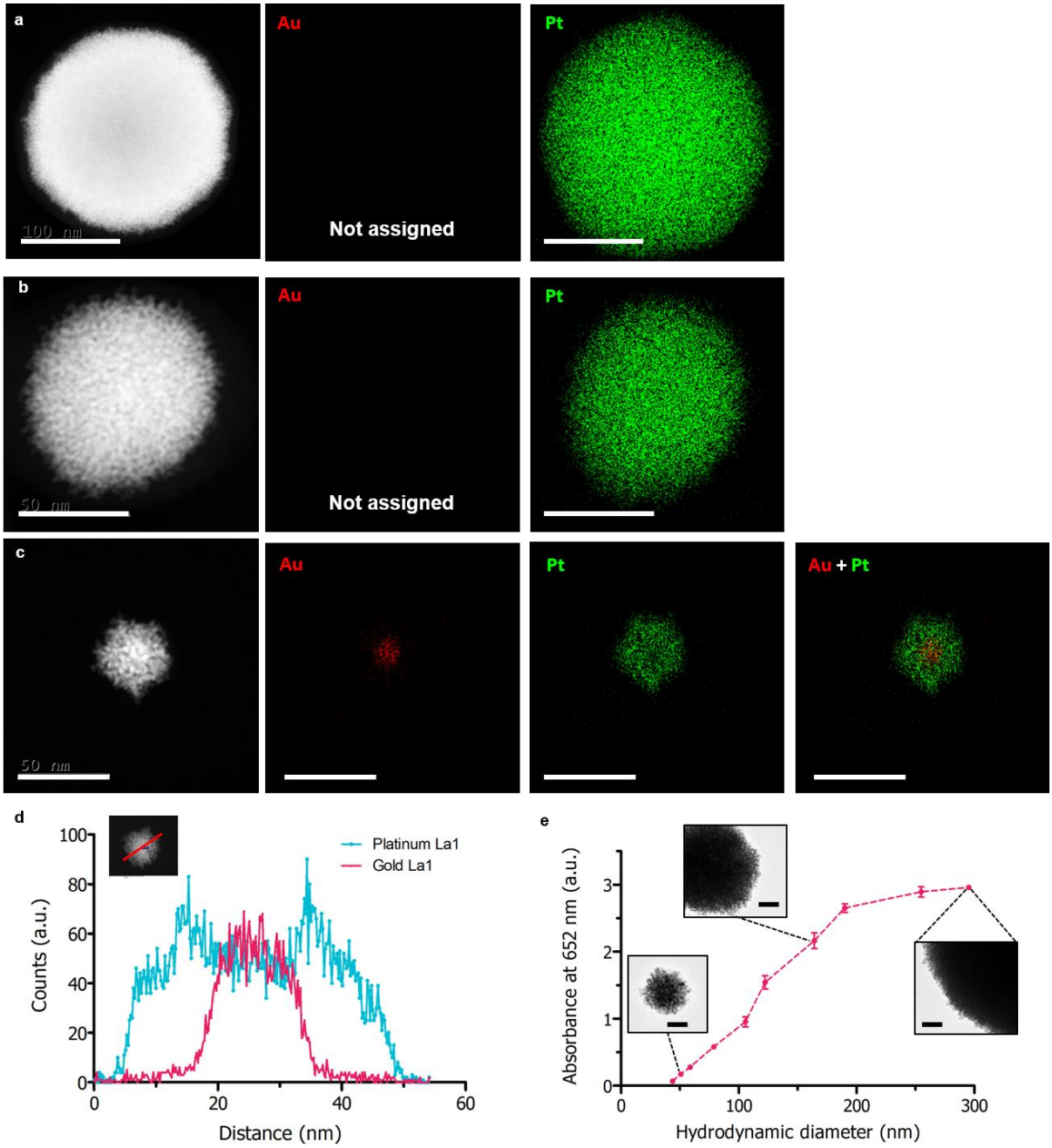

Supplementary Figure 7. Energy Dispersive X-ray (EDS) mapping of the elemental distribution of Au (red) and Pt (green) for (**a**) 200 nm (scale bar, 100 nm), (**b**) 100 nm (scale bar, 50 nm), and (**c**) 50 nm PtNCs (scale bar, 50 nm). EDS mapping reveals Au at the particle core when the Pt shell is thin (ca. 50 nm PtNC), however Au is not detected for larger 100 and 200 nm PtNCs where the Pt shell is thicker. A black box has been used to represent Au for **(a)** and **(b)** as no Au was assigned during EDS mapping analysis. For the 50 nm PtNCs, Au is clearly present in the interior (red) while Pt is distributed across the

entire particle, indicating a core-shell structure. (**d**) EDS line scan profile recorded along the central axis of an individual 50 nm PtNC further confirming core-shell structure. (**e**) Catalytic activity measured by the absorbance at 652 nm corresponding to the oxidation of TMB by H_2O_2 for PtNCs of fixed concentration and varying hydrodynamic diameter (*ca*. 50 – 300 nm). The trend in activity with increasing particle size does not scale with the external diameter surface area, indicating the availability of internal porous shell for catalytic reactions.

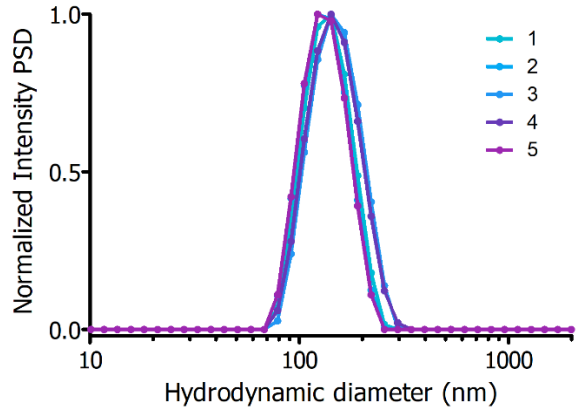

Supplementary Figure 8. Normalized particle size distribution (Intensity PSD) for five independently synthesized batches of PtNCs using the same starting seed concentration where the distributions overlap closely.

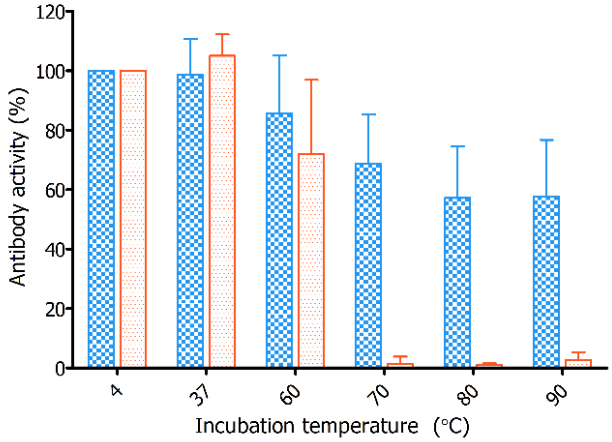

Supplementary Figure 9. Activity of 59H10 nanobody (blue) and a comparator monoclonal antibody (orange) as assessed by its ability to re-bind to p24 by indirect ELISA after 2 h

incubation at varying temperatures (4 – 90 °C). The nanobody retained at least 50% binding activity, even after incubation at 90 °C, indicating its ability to re-fold. Error bars represent standard deviation from three independent experiments.

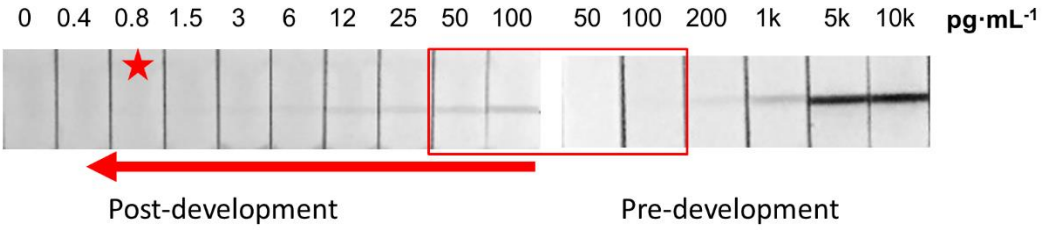

Supplementary Figure 10. Representative mobile phone images of test strips before and after catalytic development (red box highlights pre- and post- development for 50 and 100 pg·mL^{-1} samples), corresponding to varying concentrations of p24-spiked sera. Brightness in image has been increased for clarity of reproduction. The star represents the lowest concentrations distinguishable by eye.

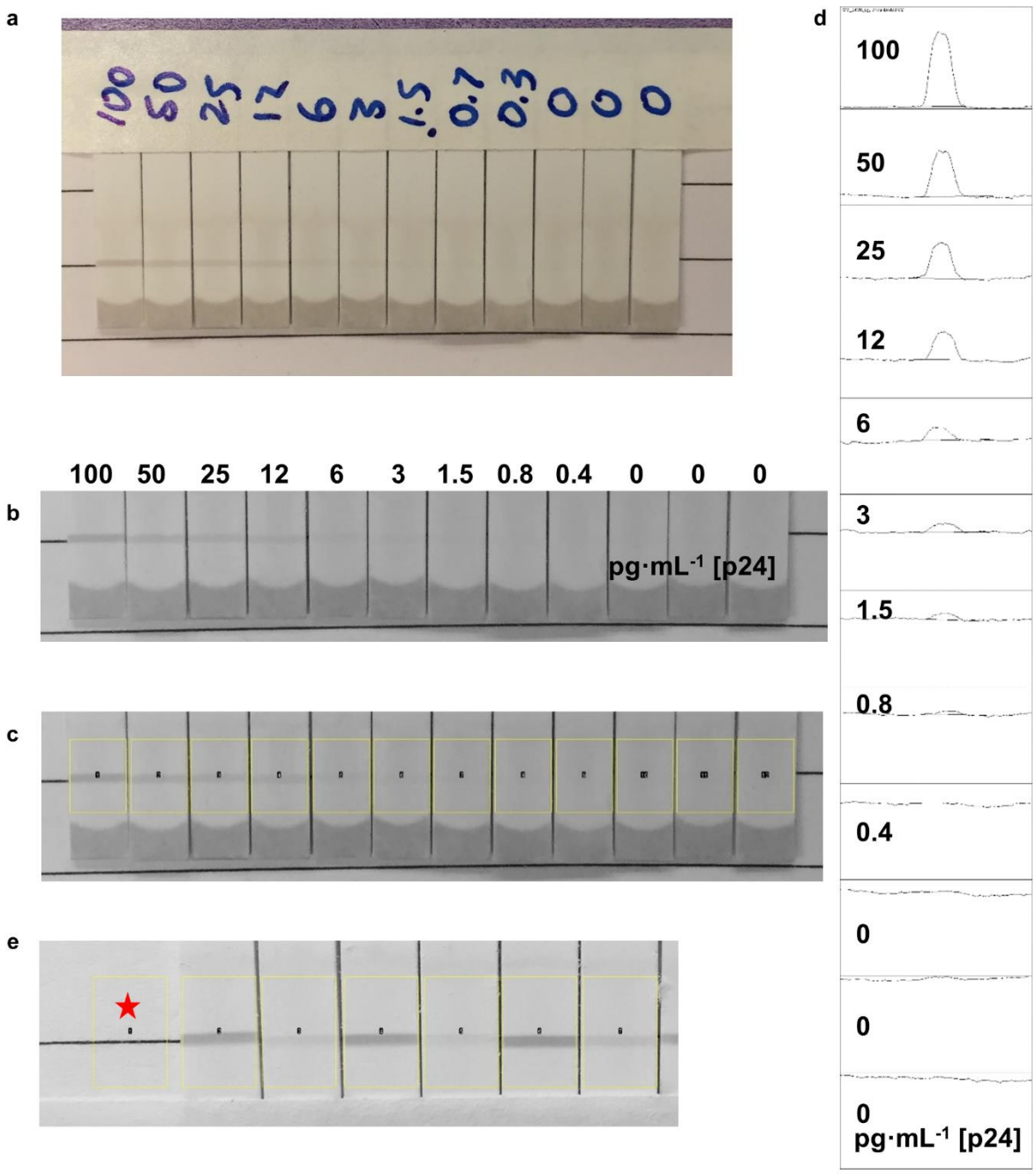

Supplementary Figure 11. Image processing procedure for analysis of LFIA strips. First, an image of the test strips was acquired using an iPhone 6 camera. Images were taken with test strips laid on the same area of a standard lab bench. One image from each independent experiment (n ≥ 3) was analyzed (**a**). Next, the image was imported into ImageJ software, and (**b**) converted to a 16-bit grayscale image. Next, using the Gel Analyzer function, rectangular regions surrounding the test line were selected (**c**). A rectangular region with a defined aspect ratio of 4:3 was used, with the width of the region spanning the test line on an

individual strip, and the height being 1.5 times the width of the test line. The selected rectangular regions were analyzed using the Gel Analyzer function in ImageJ. In brief, the profile plots of the test lines were generated (**d**), peaks of interest were defined, and then the peak areas were measured using the Wand Tool. Peak areas corresponding to “test line signal intensity” were compared between test strips within a single image. For six week accelerated aging experiment, test line intensities were normalized to a standard line (e) (highlighted by the star), which was present in all images, to account for variation in lighting between time points.

Nanobody: Methods and characterization

Synthesis general experimental

All reagents and starting materials were obtained from chemical suppliers, unless specifically stated otherwise, and were used as received. Reactions were monitored by thin layer chromatography using pre-coated SIL G/UV 254 plates purchased from VWR. Flash chromatography was carried out manually using Kiesegel 60 M 0.04/0.063 mm silica gel or automatically using a BioTage Isolera with KP-Snap or KP-Sil columns. NMR spectra were recorded using a Bruker AC300, AC500 or AC600 spectrometer (300 MHz, 500 MHz and 600 MHz respectively). Chemical shifts (δ) are given in ppm units relative to the solvent reference and coupling constants (*J*) are measured in Hertz. Proton (^{1}H) NMR multiplicities are shown as s (singlet), d (doublet), t (triplet), q (quartet), m (multiplet), dd (double doublet), dt (double triplet), etc. HMBC, HSQC and DEPT were employed to aid with accurate assignments. Infrared spectra were recorded on a Perkin Elmer Spectrum 100 FTIR spectrometer (ATR mode). High and low resolution mass spectrometry of organic molecules was provided by the EPSRC Mass Spectrometry facility at Swansea using an LTQ Orbitrap XL.

Chemical Biology General Experimental

All buffers were passed through a microfilter before use to remove particulates and the pH adjusted using 1 M HCl or 1 M NaOH. pH was measured using a Hanna Instruments pH 210 electronic pH meter. For desalting Zeba™ Spin Desalting columns, 7 KDa MWCO, were employed. Protein concentrations were determined photometrically using a Varian Cary 100 Bio UV-Visible spectrophotometer operating at 21 °C. For small scale centrifugation Eppendorf 5415 R and VWR Galaxy 14D microcentrifuges were employed. An Eppendorf Thermomixer Comfort heating block was used for temperature and agitation controlled experiments.

Non-reducing 16% acrylamide gels were made using standard procedures. A 4% stacking gel was utilised. Samples (70 µM) were mixed 5:1 with a 5× R-250 Dye SDS-loading buffer, heated for 5 minutes at 75 °C and loaded onto the gel with a total volume of 4 µL. Samples were run at constant current (30 mA) for 40 minutes in 1 × SDS running buffer and stained with Coomasie.

LCMS was performed on a Waters Acquity uPLC connected to Waters Acquity Single Quad Detector and a photodiode array. Flow rate was set at 0.600 ml/min. A Hypersil Gold C4 (50 × 2.1 mm) column at 50 °C was used for separation. Solvent A is H_2O (0.1% formic acid), solvent B is MeCN (0.1% formic acid). Mobile phase: 95:5 A:B; gradient over 4 min to 5:95 A:B. MS mode ES+; scan range: m/z ¼ 250–2,000; scan time: 0.25 s. A capillary voltage of 3.5 kV and a cone voltage of 50 V were employed. Injection volumes of 10 µl at 10 µM were used. All deconvoluted mass spectra were produced using the software provided by the manufacturer.

tert-Butyl 1-methylhydrazine-1-carboxylate[1]

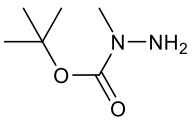

To a stirring solution of *N*-methylhydrazine (1.73 g, 37.5 mmol) at 0 °C, di-*tert*-butyl dicarbonate (8.12 g, 37.5 mmol pre-dissolved in CH_2Cl_2 (40 mL)) was added dropwise over

40 minutes. The mixture was returned to room temperature and stirred for 3 h. All solvent was removed *in vacuo* to yield *tert*-butyl 1-methylhydrazine-1-carboxylate as a clear liquid without further purification (5.00 g, 34.0 mmol, 91%). Data matched the literature. ^{1}H NMR ($CDCl_3$, 600 MHz): δ = 4.08 (br s, 2H), 3.06 (s, 3 H), 1.47 (s, 9 H); ^{13}C NMR ($CDCl_3$, 151 MHz): δ = 80.5 (CH_2), 28.5 (CH_3); IR (thin film) 3330, 3220, 2977, 2932, 1668 cm^{-1}.

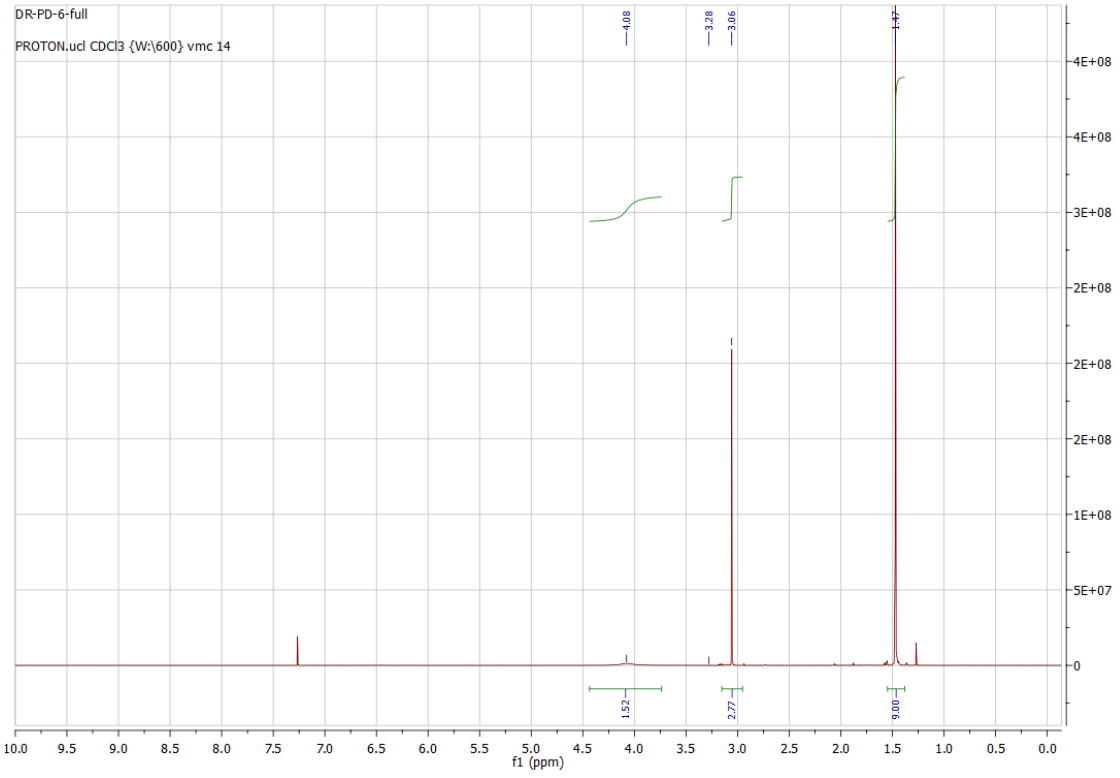

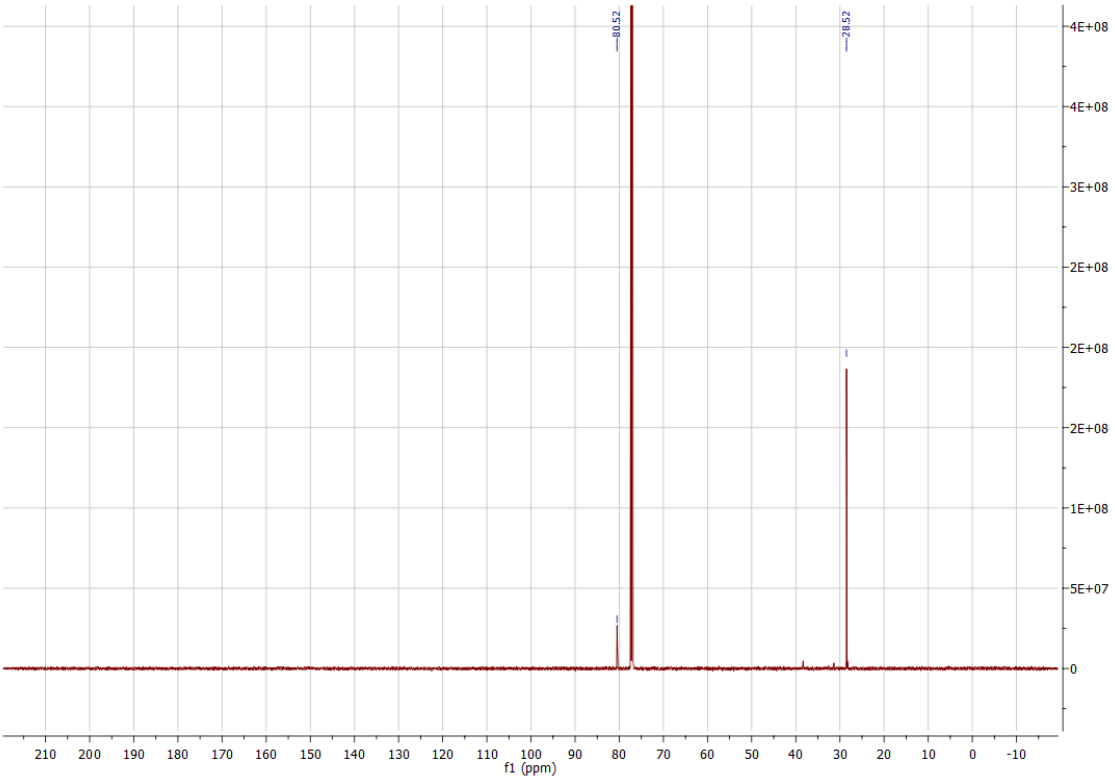

Supplementary Figure 12. ^{1}H and ^{13}C NMR data for *tert*-butyl 1-methylhydrazine-1-carboxylate.

((*tert*-Butoxycarbonyl)(methyl)amino)glycine[2]

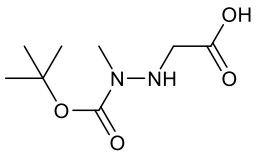

tert-Butyl 1-methylhydrazine-1-carboxylate (585 mg, 4.00 mmol) and glyoxylic acid monohydrate (368 mg, 4.00 mmol) were dissolved in *i*-PrOH (10 mL) in a round bottomed flask and stirred at room temperature for 5.5 h. 10% Pd/C (80 mg) was added and the flask placed under vacuum to remove all air. The flask was subsequently filled with an atmosphere of H_2 *via* balloon and the suspension stirred for 24 h. The solution was filtered through celite and all solvent removed *in vacuo* to yield a crude oil. Trituration with CH_2Cl_2 afforded ((*tert*-butoxycarbonyl)(methyl)amino)glycine as a waxy white solid (550 mg, 2.70

mmol, 74%). Data matched the literature. ^{1}H NMR (DMSO-d_6, 400 MHz) δ = 3.46 (s, 2 H), 2.93 (s, 3 H), 1.40 (s, 9 H); ^{13}C NMR (DMSO-d_6, 100 MHz) δ = 171.9 (C), 155.4 (C, seen by HMBC), 79.5 (C), 50.9 (CH_2), 28.3 (CH_3), 28.0 ($CH_{3)}$); IR (thin film) 3299, 2977, 2931, 1668 (br) cm^{-1}.

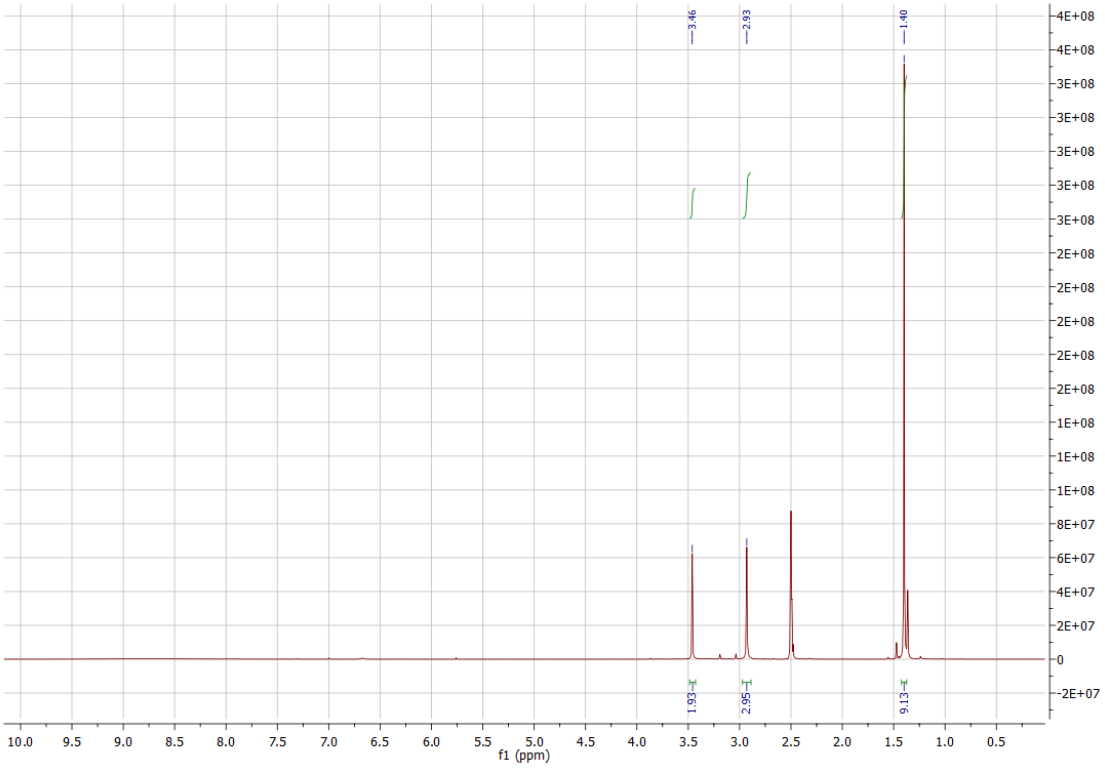

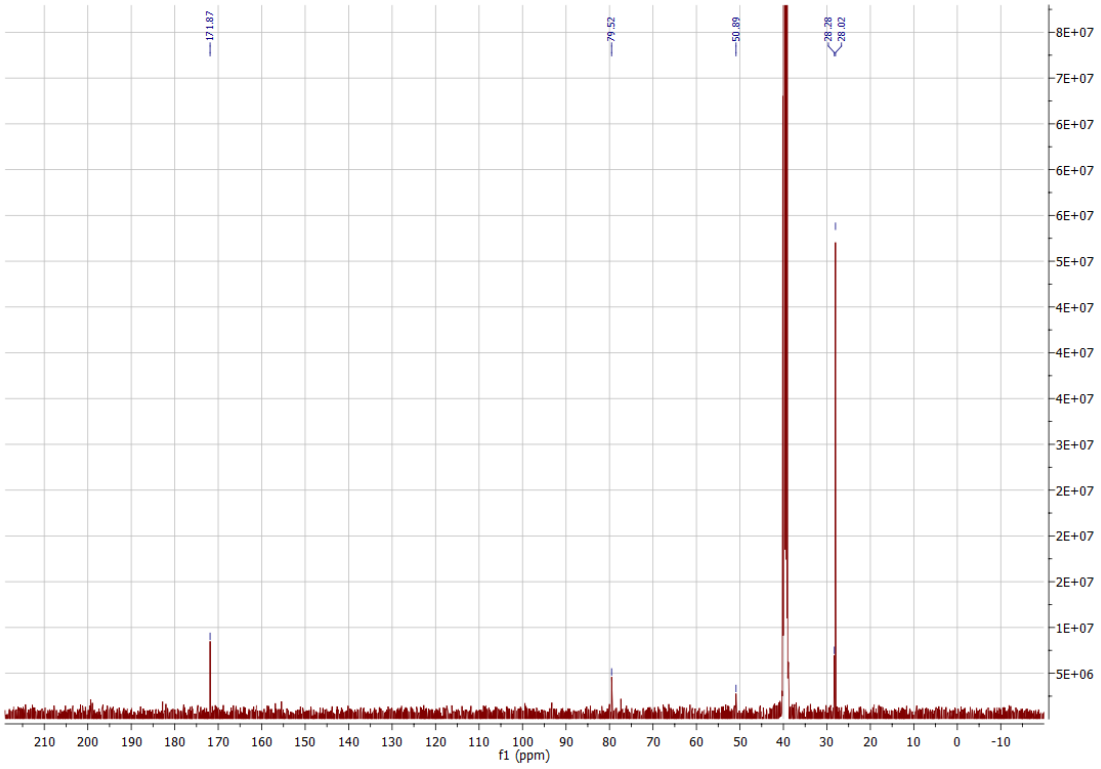

Supplementary Figure 13. ^{1}H and ^{13}C NMR data for *((tert*-butoxycarbonyl)(methyl)amino)glycine.

2-(4/5-Bromo-2-methyl-3,6-dioxo-3,6-dihydropyridazin-1(2*H*)-yl)acetic acid

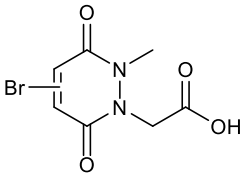

((*tert*-Butoxycarbonyl)(methyl)amino)glycine (158 mg, 0.78 mmol) and bromomaleic anhydride (138 mg, 0.78 mmol) were dissolved in acetic acid (8.5 mL) and stirred at room temperature for 2 h. After this time, the solution was heated under reflux for a further 3 h, before all solvent was removed *in vacuo*. The crude material was purified by column chromatography (1% acetic acid in acetone) to give 2-(4/5-bromo-2-methyl-3,6-dioxo-3,6-dihydropyridazin-1(2*H*)-yl)acetic acid as a waxy orange solid (134 mg, 0.51 mmol, 65%). Product was obtained as a mixture of regioisomers (4-bromo and 5-bromo).^{1}H NMR (MeOD, 600 MHz) (major regioisomer assigned) δ = 7.54 (s, 1 H), 4.92 (s, 2 H), 3.63(s, 3 H); ^{13}C

NMR (MeOD, 151 MHz) (major regioisomer assigned) δ = 170.3 (C), 157.6 (C), 154.9 (C), 136.3 (CH), 135.1 (C), 48.0 (CH_2), 34.6 (CH_3); IR (thin film) 2988, 2901, 1725, 1625 cm^{-1}; LRMS (ESI) 265 (100, $[M^{81}Br+H]^+$), 263 (98, $[M^{79}Br+H]^+$); HRMS (ESI) calc'd for $C_7H_7BrN_2O_4$ $[M^{79}Br+H]^+$ 262.9662, observed 262.9666.

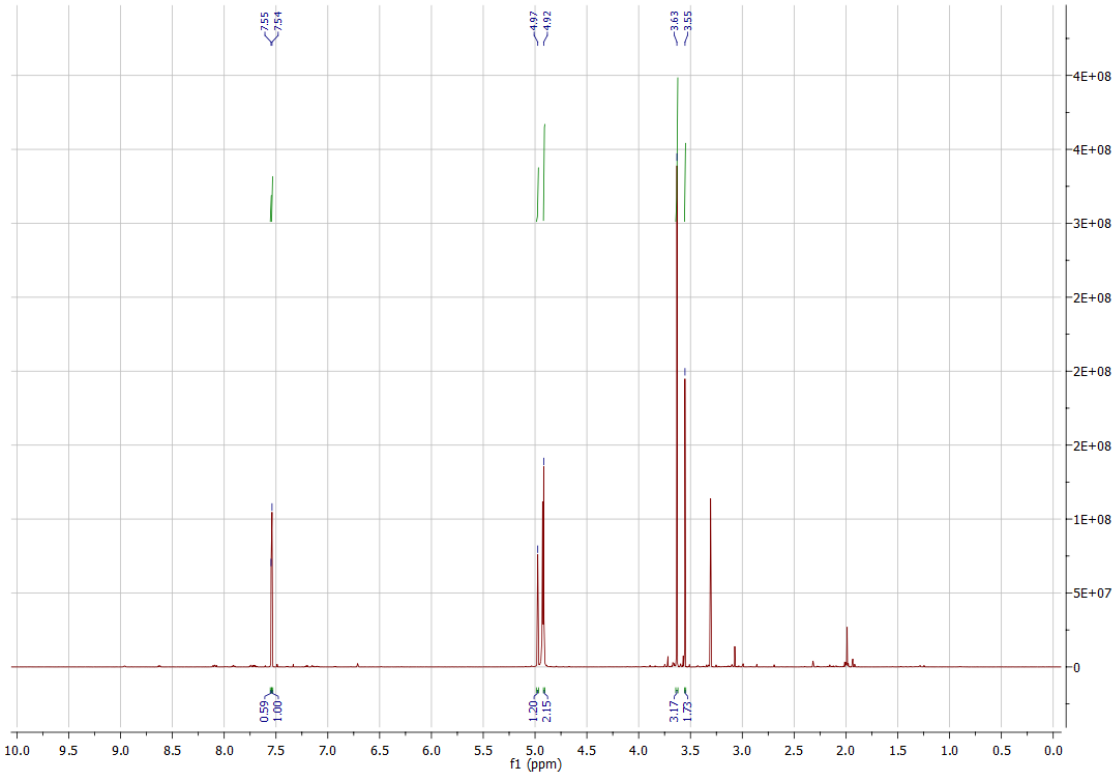

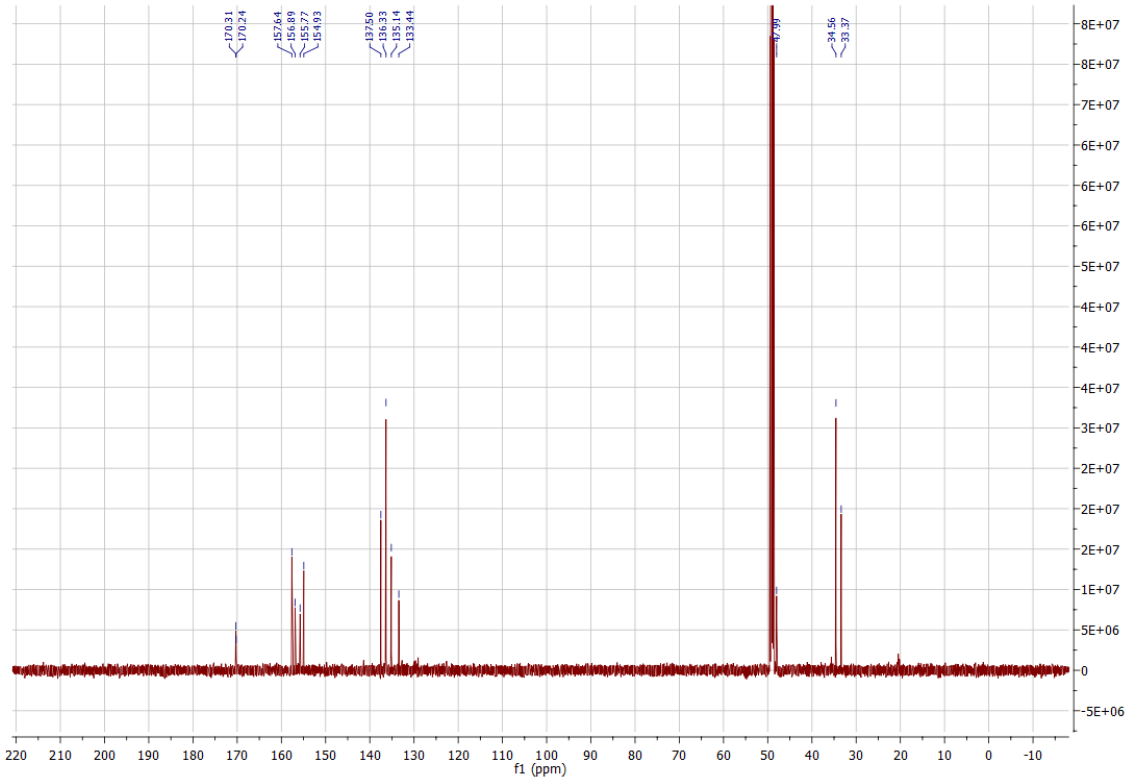

Supplementary Figure 14. ^{1}H and ^{13}C NMR data for 2-(4/5-bromo-2-methyl-3,6-dioxo-3,6-dihydropyridazin-1(2H)-yl)acetic acid.

Bromopyridazinedione-PEG$_8$-biotin

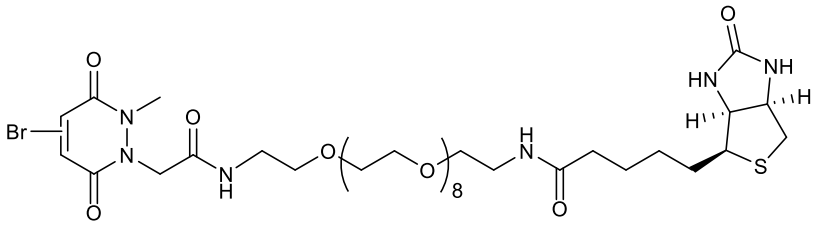

To a suspension of 2-(4/5-Bromo-2-methyl-3,6-dioxo-3,6-dihydropyridazin-1(2*H*)-yl)acetic acid (17 mg, 0.061 mmol) and HATU (61.0 mg, 0.160 mmol) in a mixture of CH_2Cl_2 (7 mL) and DMF (50 μL) was added DIPEA (22.3 μL, 0.128 mmol) and the mixture stirred at room temperature for 0.5 h. The mixture was then added to a solution of *O*-(2-Aminoethyl)-*O'*-[2-(biotinylamino)ethyl]octaethylene glycol (40.0 mg, 0.059 mmol) in CH_2Cl_2 (3 mL) and stirred at room temperature for 4 h. All solvent was then removed *in vacuo* and the crude material purified by flash chromatography (0–70% MeOH in EtOAc) to afford bromopyridazinedione-

PEG_8-biotin as a pale oil (36 mg, 0.037 mmol, 64%). Product was obtained as a mixture of regioisomers (4-bromo and 5-bromo).^{1}H NMR (MeOD, 600 MHz) (major regioisomer assigned) δ = 7.55 (s, 1 H), 4.87 (s, 2 H), 4.51-4.47 (m, 1 H), 4.30 (dd, *J*=7.9, 4.5 Hz, 1 H), 3.67-3.52 (m, 39 H), 3.45-3.41 (m, 2 H), 3.36 (t, *J*=5.5 Hz, 2 H), 3.21 (ddd, *J*=9.0, 5.6, 4.7 Hz, 1 H), 2.93 (dd, *J*=12.7, 5.0 Hz, 1 H), 2.70 (d, *J*=12.7 Hz, 1 H), 2.22 (t, *J*=7.2 Hz, 2 H), 1.77-1.56 (m, 4 H), 1.49-1.39 (m, 2 H); ^{13}C NMR (MeOD, 150 MHz) (major regioisomer assigned) δ = 176.1 (C), 168.5 (C), 166.1 (C), 157.7 (C), 154.9 (C), 137.4 (CH), 136.4 (C), 71.5-70.4 (PEG-CH_2 × 18), 63.4 (CH), 61.6 (CH), 57.0 (CH), 50.3 (CH_2), 41.1 (CH_2), 40.7 (CH_2), 40.4 (CH_2), 36.7 (CH_2), 34.6 (CH_3), 29.8 (CH_2), 29.5 (CH_2), 26.9 (CH_2); IR (thin film) 3307, 2901, 2869, 2477, 2404, 1674, 1633, 1573 cm^{-1}; LRMS (ESI) 946 (100, [M^{81}Br+NH_4]$^+$), 944 (90, [M^{79}Br+NH_4]$^+$); HRMS (ESI) calc'd for $C_{37}H_{64}BrN_6O_{14}S$: [M^{79}Br+H]$^+$ 927.3379, observed 927.3369.

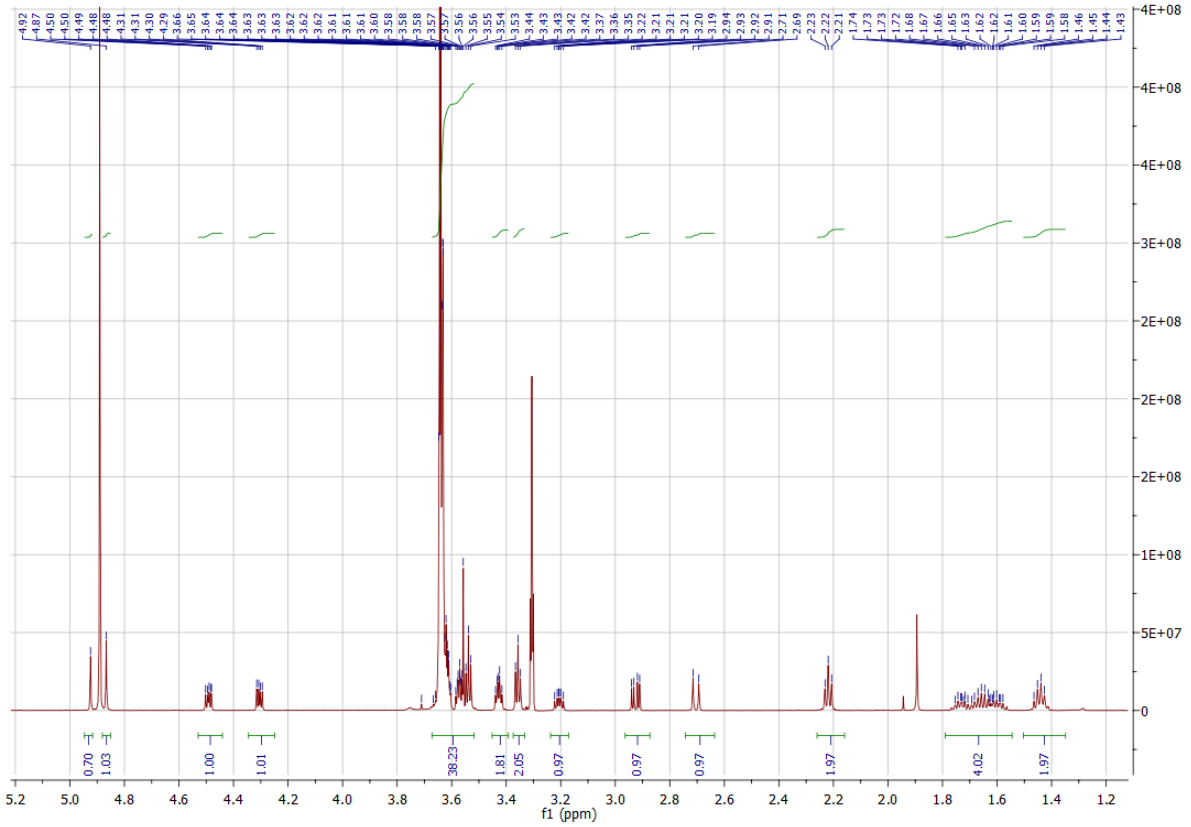

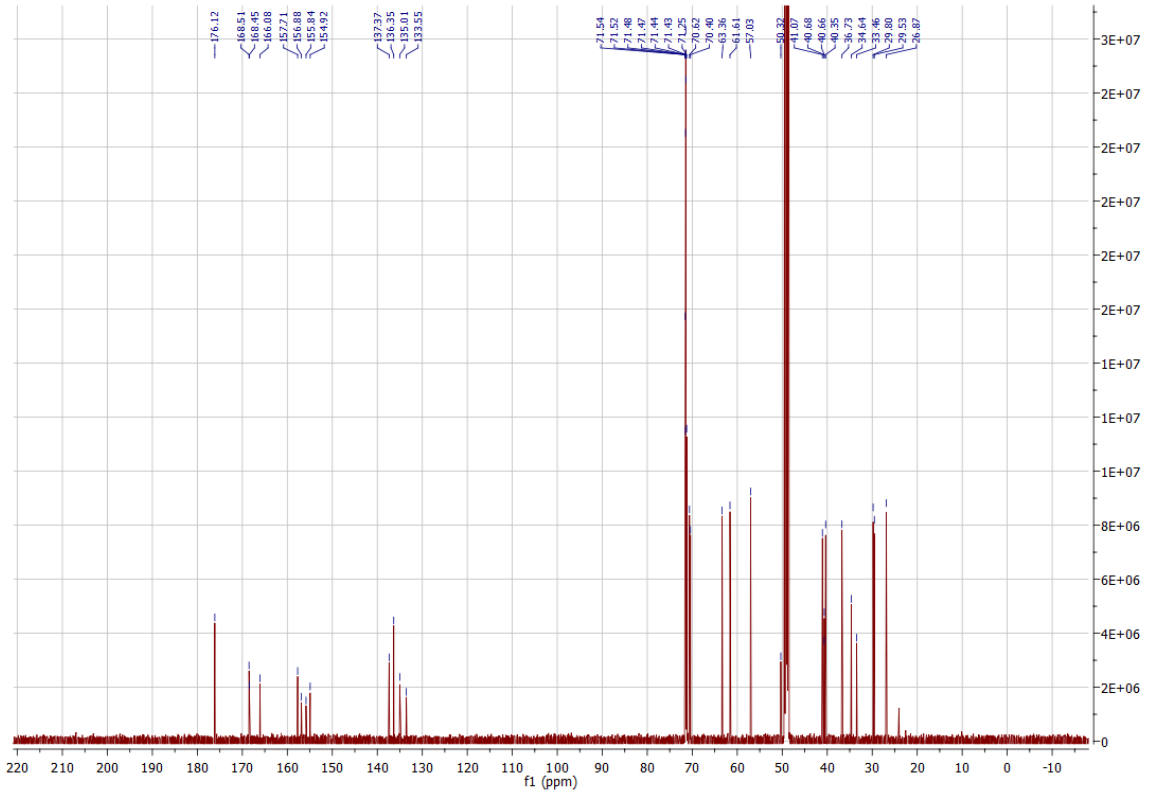

Supplementary Figure 15. ^{1}H and ^{13}C NMR data for bromopyridazinedione-PEG_8-biotin.

Biotinylation of cysteine presenting nanobody

Tris(2-carboxyethyl)phosphine HCl (TCEP-HCl) (3.8 μL, 37.6 mM in PBS pH = 7.4, 10 eq.) was added to a solution of anti-p24 nanobody (380 μL, 37.6 μM in PBS pH = 7.4) and the reaction incubated at 37 °C for 1.5 h. After this time bromopyridiazinedione-PEG_8-biotin was added (14.2 μL, 20 mM in DMSO, 20 eq.) and the reaction was incubated at 21 °C for 16 h. All small molecules were removed by desalting into PBS pH = 7.4 (Zeba™ Spin, 7 KDa MWCO, 2.00 mL, Thermo Scientific, repeated once). The volume was adjusted to 400 μL and the concentration determined photometrically to be 20.6 μM (ε_{280} = 21095 M^{-1} cm^{-1}, correction factor A_{280} for bromopyridazinedione-PEG_8-biotin = 0.28 × A_{335}). The extinction coefficient of the anti-p24 antibody was estimated using ExPASy (http://web.expasy.org/cgi-bin/protparam/protparam), using the following amino acid sequence:

MAEVQLVESGGGLVQAGGSLRLSCAASGSISRFNAMGWWRQAPGKEREFVARIVKGFDP
VLADSVKGRFTISIDSAENTLALQMNRLKPEDTAVYYCFAALDTAYWGQGTQVTVSSAAAE
QKLISEEDLNGAAHHHHHHC

Assessment of the concentration of the biotinylated anti-p24 nanobody using BCA assay (Pierce BCA Protein Assay Kit, Thermo Scientific) gave a concentration of 19.5 μM, a value in agreement with the photometric result above.

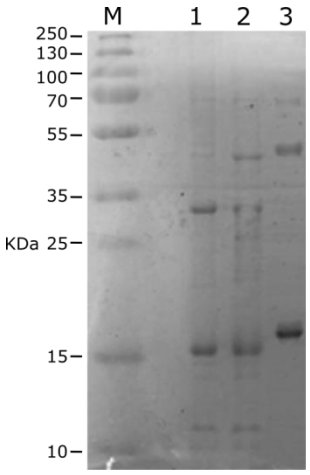

Supplementary Figure 16. M) Molecular weight marker. 1) anti-p24 nanobody non-reduced. 2) anti-p24 nanobody + 10 eq. TCEP at 37 °C for 1.5 h. 3) anti-p24 nanobody site-selectively biotinylated using bromopyridizinedionePEG_8-biotin.

(a)

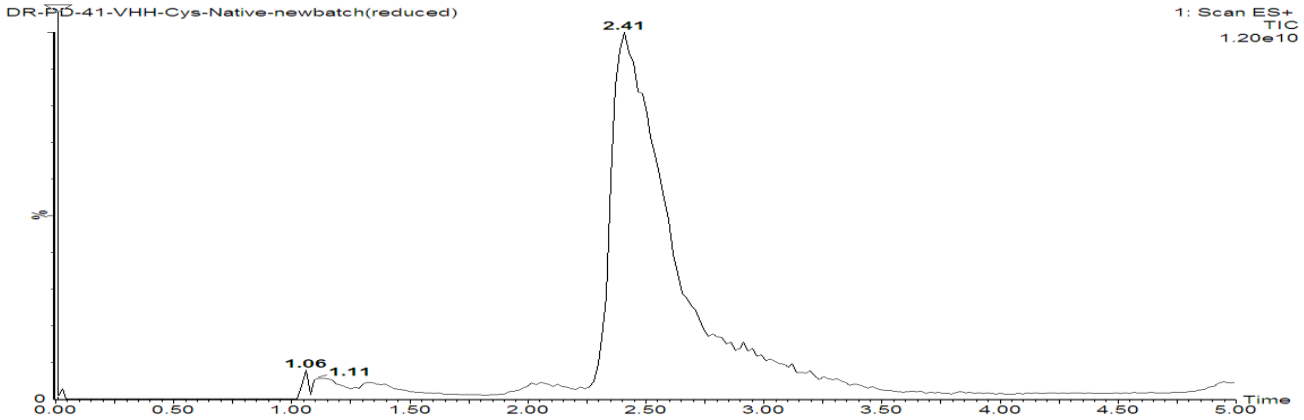

(b)

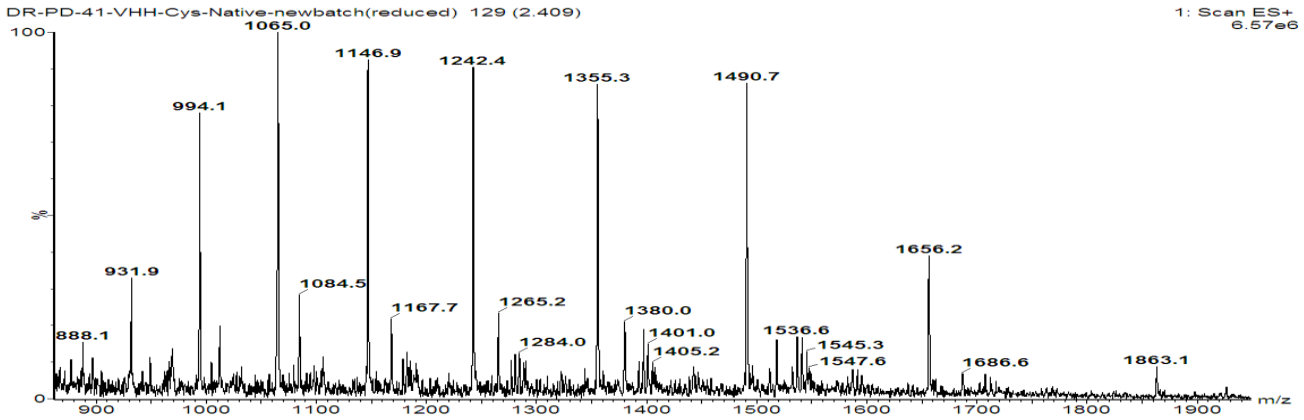

(c)

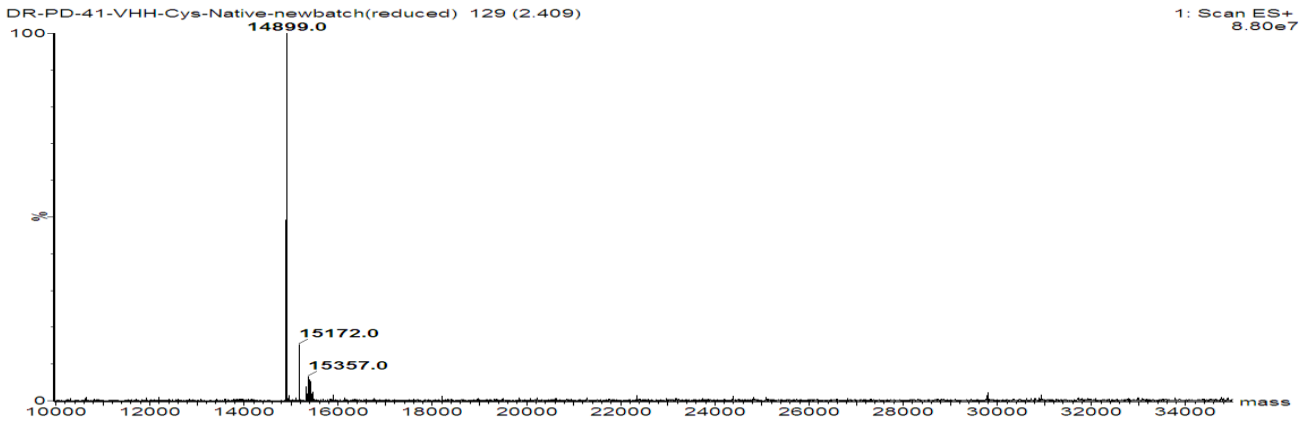

Supplementary Figure 17. (a) TIC, (b) non-deconvoluted and (c) deconvoluted MS data for reduced anti-p24 nanobody.

(a)

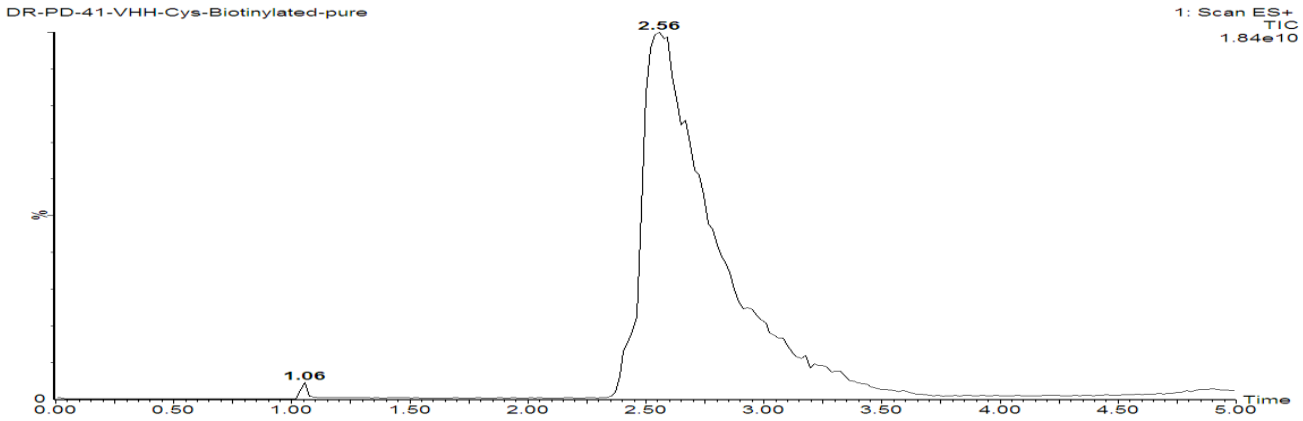

(b)

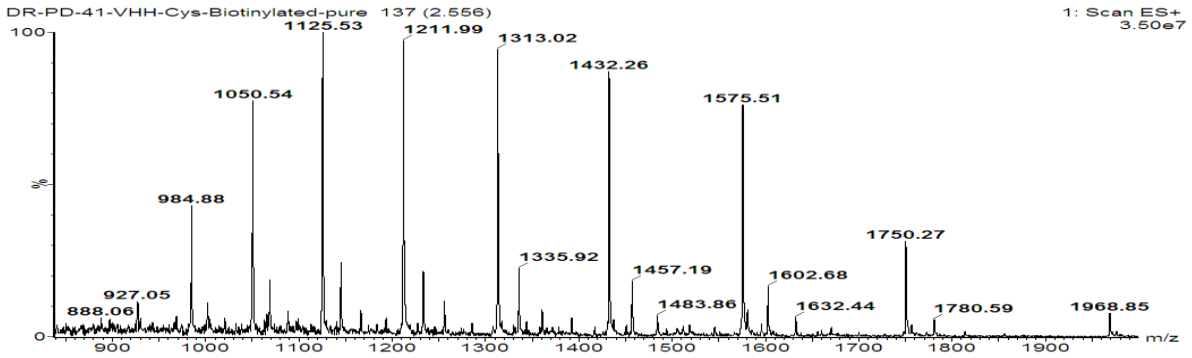

(c)

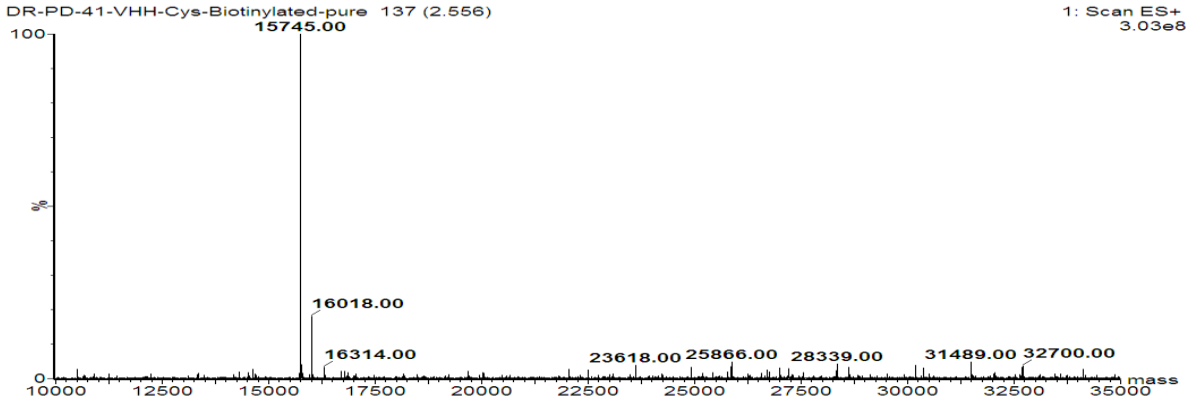

Supplementary Figure 18. (a) TIC, (b) non-deconvoluted and (c) deconvoluted MS data for site-selectively biotinylated anti-p24 nanobody.

Table 1. Affinity constants for components used in PtNC-labelled LFIA. Kinetic analysis of antibodies was performed using ForteBio instrument.

Antibody-p24 Complex	**K_D (M)**	**k_{on} ($M^{-1}s^{-1}$)**	**k_{off} (s^{-1})**
Nanobody	2.0×10^{-9}	1.6×10^{5}	4.3×10^{-4}
Nanobody-biotin	3.0×10^{-9}	1.6×10^{5}	4.0×10^{-4}
Capricorn 1/2	2.1×10^{-9}	4.3×10^{4}	2.4×10^{-4}

References

1 K. Hasumi *et al*., *Bioorg Med Chem*, 2014, **22**, 4162–4176.s

2 J. Schmitz *et al.*, *ACS Med. Chem. Lett*, 2014, **5**, 1076–1081.